Earthq Eng & Eng Vib (2021) 20: 605-620 **DOI**: https://doi.org/10.1007/s11803-021-2041-8

Matrix test measurements of ground-borne vibration induced by the heavy-duty trains on embankment and cutting tracks in a loess area

Xie Qiang[1†], Wu Zhi-Hui[1‡], Dong Jie[2†] and Zhong Shuai[2§]

1. *School of Civil Engineering, Chongqing University, Chongqing 400045, China*

2. *College of Civil Engineering, Hebei University of Architecture, Zhangjiakou 075000, China*

Abstract: This paper presents a comparative analysis of ground vibration in three directions generated by a heavy-duty railway with various track sections. The vibration characteristics in the plane area were investigated by using matrix test measurements. Acceleration peak attenuation was faster within 25 m from the embankment, and the high-frequency vibration attenuates faster with increased distance. For the cutting section with multi-stage soil slope, decay rate of acceleration was relatively larger. The acceleration level of the plane region ranged to 82.2–89.1 dB by the single C80 train. Yet the acceleration level caused by the C80 trains running parallel after meeting showed a distinct increment. The increment of the cutting section was much larger compared with the embankment section, with the increment ranging from 1.2–2.5 dB. In terms of the cutting section, *Y* direction acceleration was dominant closer to the track. Within 10–30 m of the track, the *Y* direction acceleration (perpendicular to the rail) decreased rapidly and became comparable to the *X* direction (parallel to the rail) and *Z* direction. Additionally, the cutting case generated a higher level of vibration in all three directions compared to the embankment, but as the distance from track increased, the deviation between acceleration gradually decreased.

Keywords: heavy-duty railway; different track sections; field measurement; vibration response characteristics; cutting slope

1 Introduction

Heavy-duty railways are extensively employed in many countries due to transport capacity, low cost and high efficiency. The railways inevitably cross mountains and plains. With the increasing scale of the railway industry, axle load and the traction weight of heavy-duty trains continue to increase, which causes significant vibration increase for a heavy-duty railway. Due to the long duration, continuous cycles, and large influence range of heavy-duty railway vibration, the negative environmental effect is becoming more serious (Connolly *et al*., 2016). Railway vibrations can cause significant negative effects such as personal distress near building structures and causing soil slope damage. So, the impact of vibrations caused by heavy-duty trains has recently received widespread attention. In a loess area of the north China, there are many heavy-duty railways, such as Daqin Railway, Shuohuang Railway, and Tanghu Railway. These heavy-duty railways cause a serious impact on the surrounding geological environment.

In the research that has been done on the environmental vibration caused by the railways, many scholars have regarded train excitation load to be equivalent to axles load (Karlström, 2006) and random dynamic loads (Lu *et al*., 2006), and have considered a complex calculation procedure system to study vibration response characteristics (Sheng *et al*., 2003; Xia *et al*., 2010; Wang *et al*., 2017). Some scholars have established a calculation procedure model by considering rails, sleepers, ballast layers and foundations (Sheng *et al*., 1999; Cao *et al*., 2011). A new "periodic configuration update" (Mezeh *et al*., 2017) numerical method has been applied to solve the problem of a vertical harmonic load, which serves as the basis for the study of track-ground vibration. In addition, some scholars have studied vibration displacement (Koroma *et al*., 2017; Picoux and Houédec, 2005), vibration acceleration (Auersch, 2006) and vibration velocity (Germonpré *et al*., 2017; Degrande and Schillemans, 2001; Lombaert *et al*., 2014) of the ground along railways.

Some scholars have proposed a numerical simulation model to analyze dynamic response. Based on the two-dimensional finite element method, the boundary element method (Galvín and Domínguez, 2007) and the finite difference method (Zhang *et al*., 2016), the

Correspondence to: Dong Jie, College of Civil Engineering, Hebei University of Architecture, Zhangjiakou 075000, China
Tel: +86-15222783120
E-mail: dongjie1003@hotmail.com
[†]Professor; [‡]PhD Student; [§]Graduate Student

Supported by: Natural Science Foundation of China under Grant No. 51878242 and Hebei Natural Science Foundation of China under Grant Nos. E2017404013 and E2020404007
Received July 22, 2019; **Accepted** January 7, 2021

numerical model was established to analyze the dynamic characteristics of tracks under train loads. Alves Costa *et al*. (2012) and Yang *et al*. (2003) established a train-track-foundation 2.5D numerical model to further investigate the vibration propagation law and vibration frequency domain characteristics of high-speed trains. Subsequently, most scholars have studied the variation characteristics of acceleration (Sun *et al*., 2016), vibration velocity (Correia dos Santos *et al*., 2017) and the vibration level (Kouroussis *et al*., 2014) of a railway by establishing a three-dimensional numerical model. An efficient three-dimensional dynamic track-subgrade interaction model (Gao *et al*., 2018) was established and then validated by field investigations.

Field measurement research can objectively reflect vibration level and provide effective verification for a numerical simulation. Based on high-speed railway field tests, Connolly *et al*. (2014) explored the influence of different subgrade structures on the vibration velocity of surrounding ground. Combined with field measurement and numerical simulation, Gao *et al*. (2017) studied railway track dynamic behavior near critical speed. Taga *et al*. (2015) investigated the cut slope stability problems while considering dynamic loading. Zhai *et al*. (2015) analyzed ground acceleration and vibration frequency characteristics by using field measurements. Feng *et al*. (2017) conducted field tests on different subgrade forms to explore the variation law of three-direction acceleration regarding surrounding ground. By use of a large-scale field test, ground vibrations (Correia dos Santos *et al*., 2016), due to different passing trains and the characteristics and uncertainties of railway ground-borne vibration prediction (Connolly *et al*., 2015), were further explored. Li *et al*. (2018) investigated the dynamic response of the mountainous high-speed railway subgrade. Based on the field-measured data, some scholars conducted additional research on dynamic characteristics, such as vibration acceleration and velocity over a distance along a railway (Ling *et al*., 2009; Xia *et al*., 2009; Zhai *et al*., 2010; Dong *et al*., 2019).

The existing research on train-induced vibration has mainly concentrated on high-speed railways and general freight railway in plain areas. In the present studies, some investigations have studied vibrations of heavy-duty embankment tracks with increasing height (Li *et al*., 2017). Some researchers have focused on the dynamic stress in subgrade under larger axle loads. In mountainous areas, studies on ground vibration characteristics at the slope surface are scarce.

A review of the research literature with regard to the vibration induced by heavy-duty trains shows that a comparative analysis of ground vibration under heavy train loads between an embankment section and a cutting section with multiple-steps slopes has not done, in particular, any deviation analysis of acceleration levels in three directions. In addition, much more attention has been paid to the vibration attenuation law, perpendicular to the track, based on linear test points. The research relating to vibration characteristics in the plane region near the heavy-duty railway line is insufficient. It is necessary to study the vibration response of the plane region by matrix test measurements near heavy-haul railways. Additionally, the vibration rules of different railway sections should be further investigated. Based on the research done about heavy-duty railway surroundings vibration in the loess area, it is expected to provide a reference for the construction and planning of villages and along heavy-duty railways in plains areas. This also can provide guidance for the design of the railway line and the safety of soil slopes in mountainous areas.

With the increase of heavy-duty freight railways, train-induced vibrations will cause a significant negative impact on the geological environment and the development of urbanization. Therefore, research on vibration characteristics along heavy-duty railways is essential. The present study selected the Daqin Railway and Shuohuang Railway in the north China plain loess area. Figure 1 presents the geological conditions and the location of the study area. The paper presents a field experiment done on different track sections, combining a train-track-ground model to analyze the influence of a heavy-duty railway on near ground vibration. First, the matrix test measurements were arranged to collect vibration acceleration. Then the acceleration attenuation character with distance, the main vibration-affected area, the vibration amplitude and the vibration level of the near plane region were primarily investigated. Additionally, taking the embankment section and the cutting section in mountainous area as objects, we further researched the deviation characteristics of vibration in three directions with heavy-duty train loads.

2 Field test

2.1 Measuring point arrangement

2.1.1 Site 1 Embankment track

Site 1 is located in Yuanping City, which is located on a plains area. The loess distribution is uniform. The railway test section primarily consists of an embankment, as shown in Fig. 2(a). The embankment is composed of a 0.6-m-thick gravel ballast layer, a 0.5-m-thick subgrade and a 3.0-m-thick embankment body with sand clay. The embankment has a slope of 1:1.5. The plane matrix test measurements are set up in the near-field area within 25 m to the embankment, a total of 12 measuring points. The linear test points A1–A6 are arranged with distances of 5 m, 15 m, 25 m, 35 m, 45 m, and 55 m from the embankment foot. Among them, the three direction sensors are arranged for A1 – A4; the others are the vertical direction sensors, as shown in Fig. 3(a).

2.1.2 Site 2 Cutting track

Site 2 is located in the town of Huashaoying in a

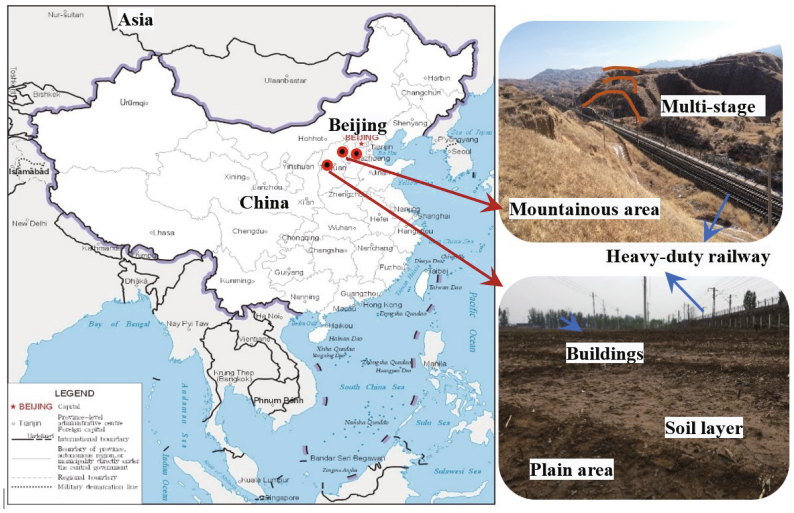

Fig. 1 Location of the study sites in a loess area

(a) Embankment track configuration (b) Cutting track configuration

Fig. 2 Overview of different site sections

mountainous area, where the distribution of surface loess is relatively uniform. The track section configuration is shown in Fig. 2(b). The track configuration consists of a cutting with a slope rate of 1:1.5. The three direction sensors are arranged for M1 – M4, where *X* is the direction parallel to the rail, *Y* is the direction perpendicular to the rail, and *Z* is the vertical direction. The vertical direction sensors are arranged in points M5 – M8, as shown in Fig. 3(b).

2.2 Test instrument

The acceleration test system used a cDAQ-9174 produced by the NI, which is a multichannel parallel data acquisition system. The CT1100 LC (vertical direction) acceleration sensors are adopted, with a voltage sensitivity of 1000 mv/g, an acquisition range of -5–5 g, and a frequency of 0.2–1600 Hz. Additionally, CT1100 LS (three directions) acceleration sensors are adopted, with a voltage sensitivity of 2000 mv/g, an acquisition range of -2.5 –2.5 g, and a frequency of 0.2–1000 Hz.

2.3 Train information

The monitoring trains include the C80, C70 and C64K full-load models. The axle load of the full-load C80 train is 25 t with a running speed ranging from 60–75 km/h; the C70 train is 23 t with a running speed from 50–71 km/h; and the C64K train is 21 t with a running speed from 48–61 km/h. Detailed train information is shown in Table 1.

3 Analysis of field test results

3.1 Attenuation of vibration acceleration

Based on typical heavy-duty trains (C80 trains with a speed of 70.8 km/h, C70 trains with a speed of 70.9 km/h and C64K trains with a speed of 61.1 km/h), the vibration attenuation that is perpendicular to the railway during train running was investigated. Figure 4 shows

the *Z*-direction acceleration time-history at A1 for full-load trains about C80, C70 and C64K.

Figure 4(a) shows that the acceleration-time history curve can clearly reflect the train groupings and the relative positions of the bogie pairs, which cause distinct vibration peaks and contain a series of periodic waveforms. The vibration response caused by a C80 train is intense, and acceleration peaks of A1, which correspond to the C80, C70, and C64K trains, are 0.013 g, 0.011 g and 0.009 g, respectively. Long-time vibration increases dynamic response amplitude near the railway, which increases the harmful impact on surrounding buildings, as well as the level of human comfort.

Figure 5(a) illustrates the fitting curves of the *Z*-direction acceleration peak. The acceleration peak rapidly decays within 5–25 m from the embankment, and the attenuation rates for C80, C70 and C64K trains are 53.1%, 61.8%, and 48.8%, respectively. In a far field, 25 m away from an embankment, the attenuation trend of the acceleration peak gradually slows as distance increases, and acceleration peaks in a region 55 m from the embankment are attenuated by 69.9%, 68.2% and 64.4%, respectively.

As shown in Fig. 5(b), the curve shows the average value of the *Z*-direction acceleration peak for cutting track in a mountainous area. The acceleration peak rapidly decays within 30 m for all trains. In an area 30 m away from the track, the attenuation trend of the acceleration peak gradually slows with distance. At the top of the first grade slope, the acceleration decay rate is up to 70% for a C80 train. At the M7 point, the slope footing of the third grade slope, the acceleration decay rate is 88%. This may be due to the space height of the cutting section changes relative to the embankment section, and that the decay rate of vibration acceleration is larger.

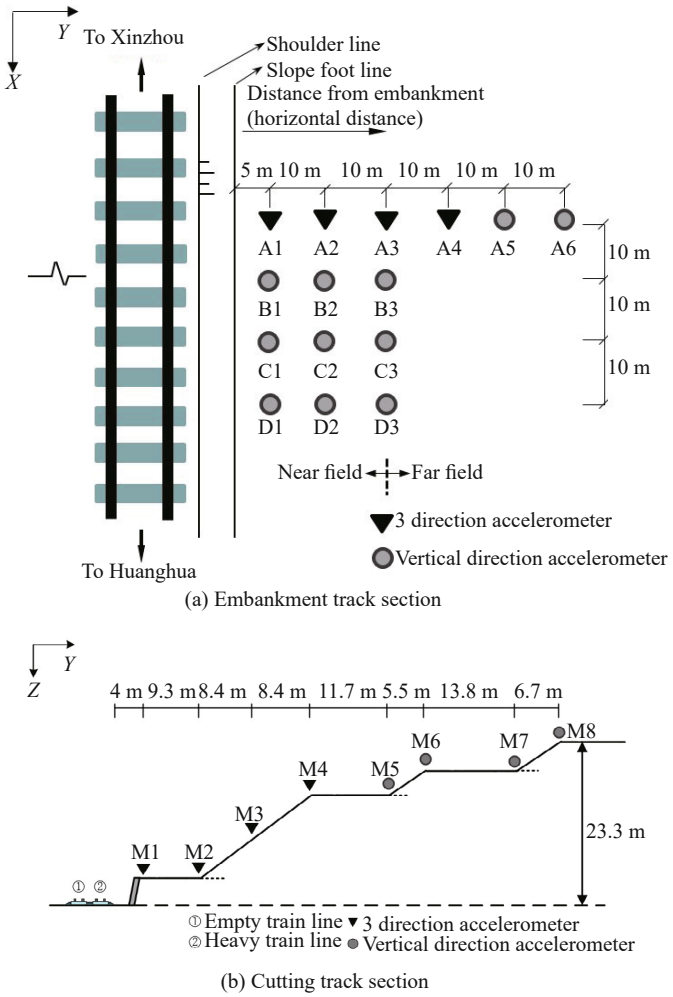

Fig. 3 Schematic diagram of accelerometers setup

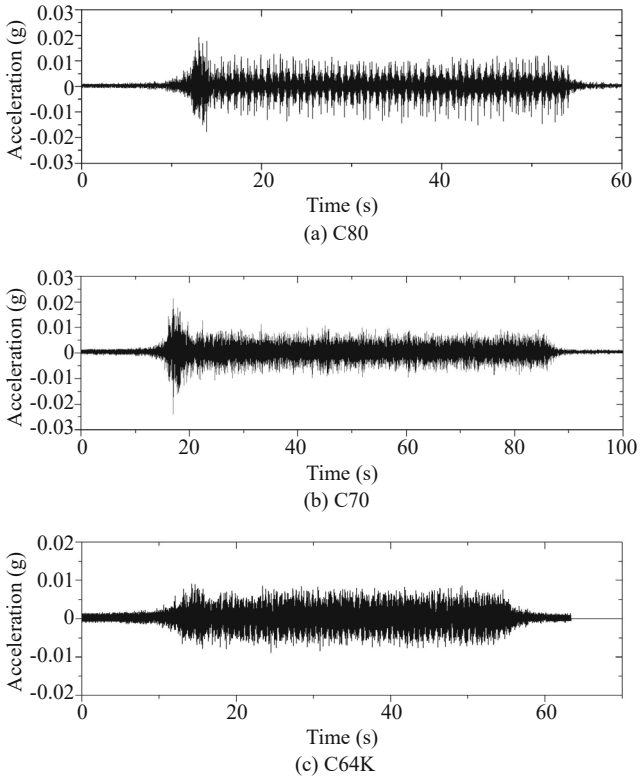

Fig. 4 Time - histories of the accelerations induced by trains

Table 1 Information on three types of trains

Number	Train type	L_a (m)	L_b (m)	Length (m)	Axle load (t)
1	C80	3.8	8.2	12	25
2	C70	4.7	9.2	13.9	23
3	C64K	4.7	8.7	13.4	21

Note: L_a - Distance between the bogies on the carriages; L_b - Distance between the bogie centers

3.2 Acceleration response characteristics within a plane

By comparing and analyzing the acceleration amplitude of the rectangular test array that is caused by different heavy-duty trains, the vibration response, the characteristics of the near-field region around the railway during train running is investigated.

Figure 6 shows the results of the plane matrix test in the near-field region. The C80 train caused the strongest vibration response in the near-field region. Within 5–25 m from the embankment, the acceleration caused by the C80 train ranges from 0.13–0.055 m/s^2, the acceleration caused by C70 ranges from 0.12–0.045 m/s^2, and the acceleration caused by C64K ranges from 0.085–0.030 m/s^2. Furthermore, the acceleration amplitude of the same row in the same distance from the embankment is inconsistent, which may be caused by a heterogeneous body due to the specific structural nature of the site soil layer.

Figure 7 shows the frequency domain characteristics of the acceleration from different trains. As the propagating distance increases, the high-frequency portion attenuates faster compared with the low-

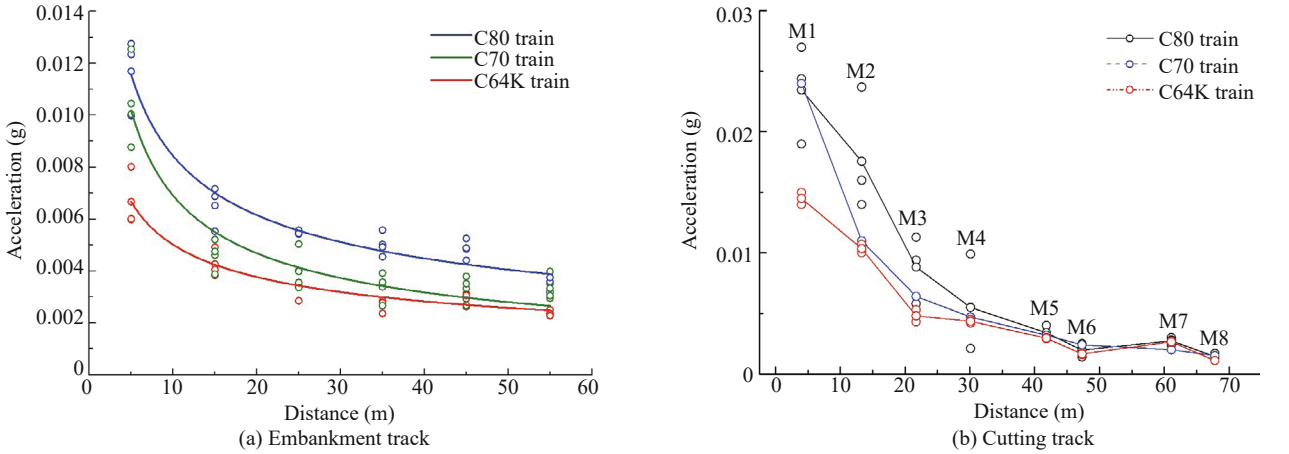

(a) Embankment track (b) Cutting track

Fig. 5 Vibration attenuation characteristics for different sections

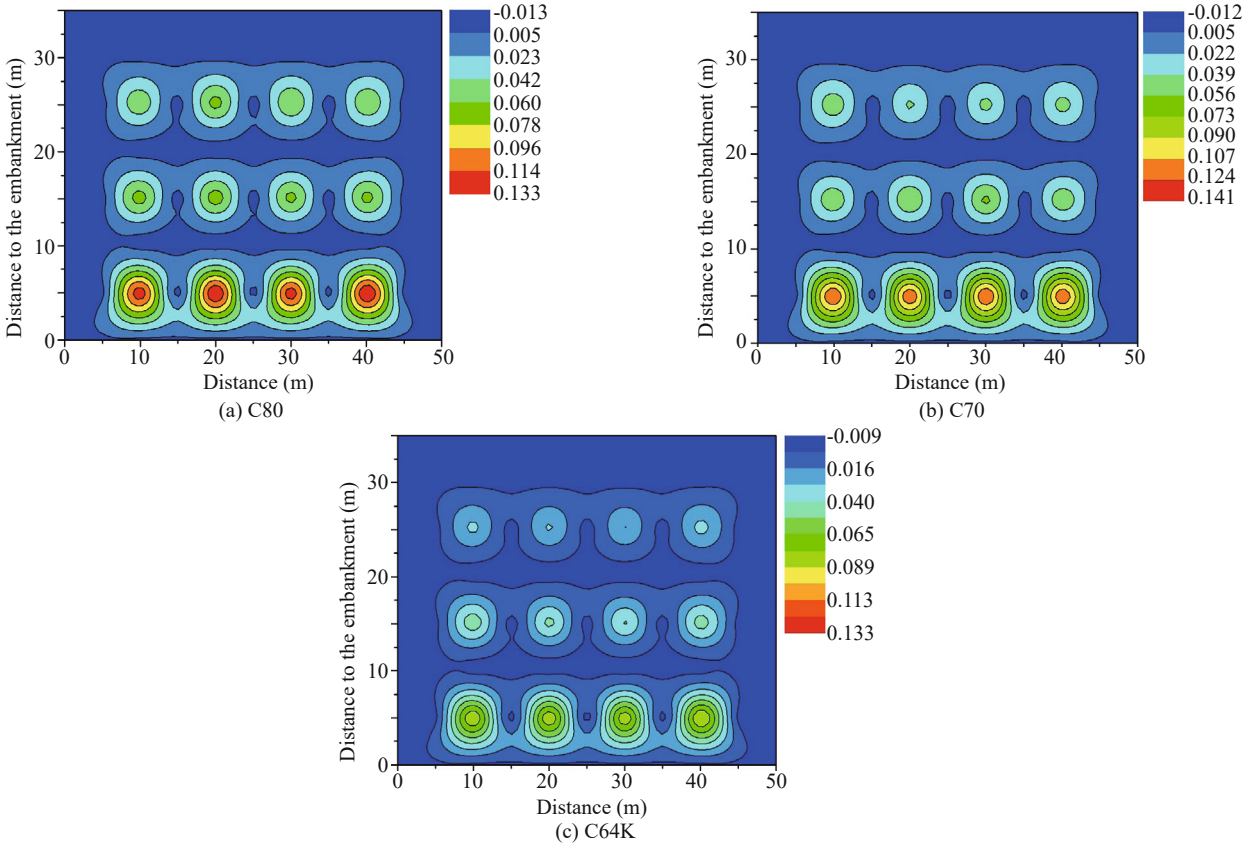

(a) C80 (b) C70

(c) C64K

Fig. 6 *Z*-direction acceleration in near-field

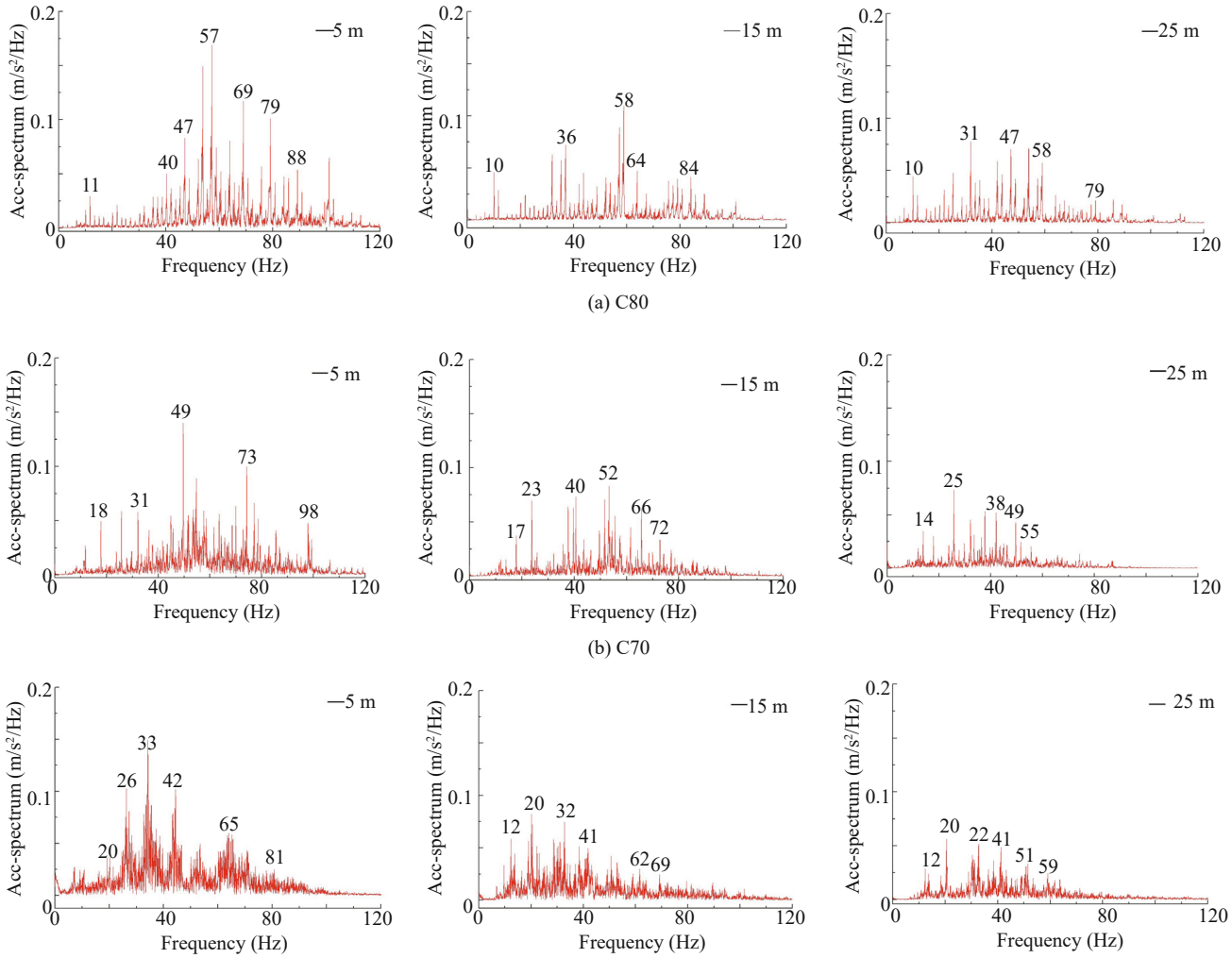

Fig. 7 The acceleration spectra from different trains

frequency portion. Similarly, the vibrational energy of the frequencies continues to decay as distance increases. At an area close to the track, the vibrational energy contains abundant high-frequency components, and fewer high-frequency vibrations occur at distances more than 25 m from the track. Due to the dissipation of high-frequency energy in the soil medium, high-frequency vibrations disappear faster, so the vibration energy with high frequency will not propagate outward.

In addition, the dominant frequency of the vibration contains the most vibration energy, in the 5m area from the track. The frequency band of the vibration caused by the C80 is mainly distributed between 10–88 Hz, and the frequency bands are 18–98 Hz and 20–81 Hz, corresponding to the C70 and C64k. Moreover, in the 15m area from the track, the frequency bands are mainly distributed between 10–84 Hz, 17–72 Hz and 12–69 Hz for different trains. In the 15m area from the track, the frequency bands are mainly distributed between 10–79 Hz, 14–55 Hz, 12–59 Hz, respectively. As the distance between the measuring points and the track increases, the high frequency vibration will attenuate significantly, affected by the surrounding soil condition, and the high frequency part of the dominant frequencies vibration will decrease correspondingly.

3.3 Vibration level within plane

The vibration acceleration level is used as the evaluation index for the vibration intensities in different areas. Figure 8 shows the vibration level characteristics in the near field that are caused by one-way trains and the C80 trains that are parallel running after meeting.

As shown in Fig. 8, the acceleration level obviously attenuates with the increase in distance in plains area. When a single C80 train runs, the acceleration level in the near-field region ranges from 82.2–89.1 dB, and the acceleration levels range from 81.2–86.9 dB and 80.3–84.4 dB, induced by the C70 and C64K trains. The vibration level caused by the C80 train running parallel after meeting exhibits a distinct increase in amplitude, due to the larger impact load on the track. The analysis indicates there is a serious vibration problem in the near-field region, caused by different heavy-duty trains

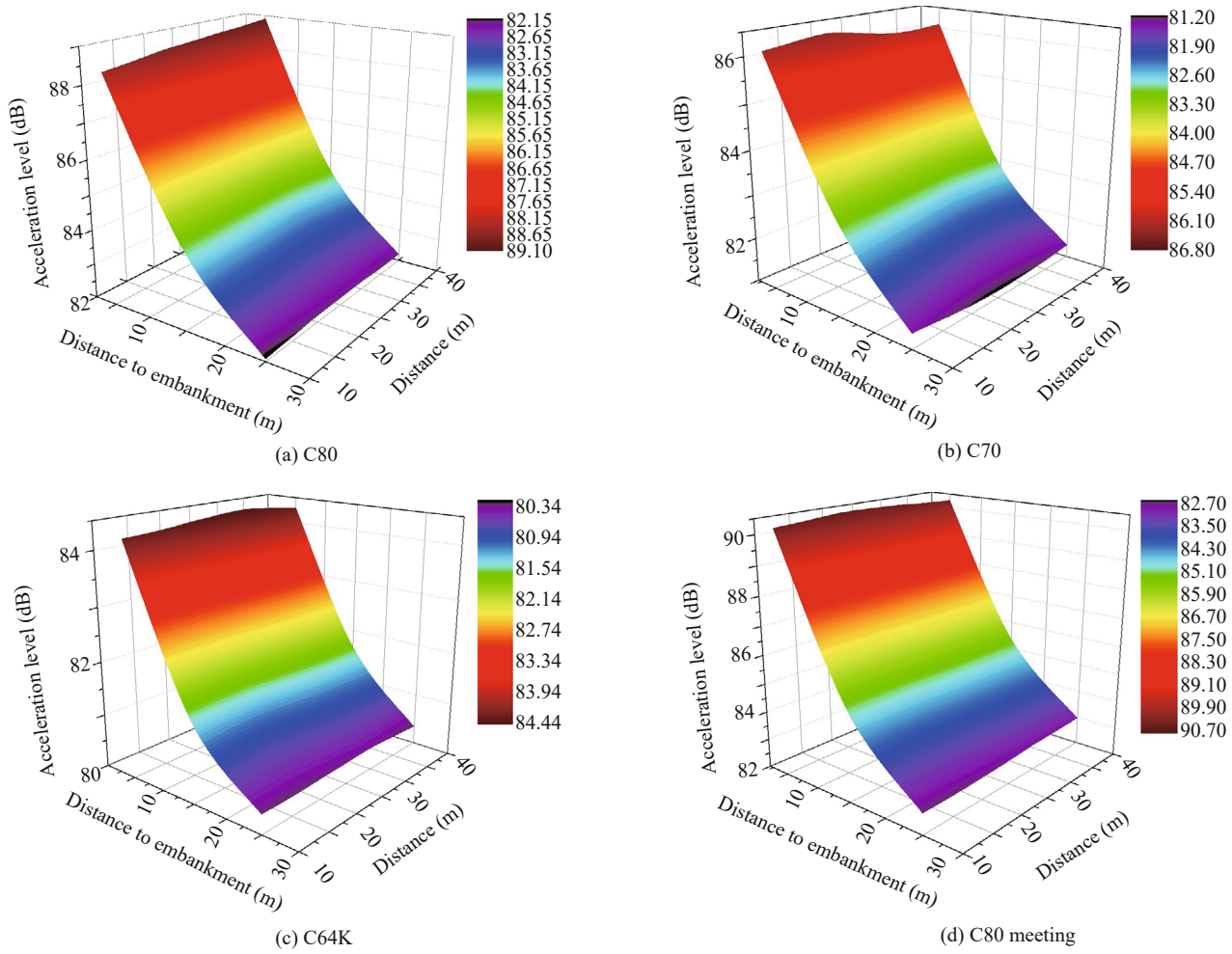

Fig. 8 *Z*-direction acceleration level in near-field

running. This is especially true when the railway passes through sensitive areas, such as a buildings region, and therefore some vibration isolation measures must be taken to mitigate the vibration effects.

3.4 Vibration effect area induced by trains

Figure 9 reflects the main vibration-affected areas caused by the C80, C70 and C64K. The *Z* direction vibration amplitude is larger and the vibration response is intense in the range of a 25–30 m area beside the railway. The running C80 train caused a larger vibration response on the surrounding environment within 85 m in front of the running train. The C64K and C70 trains have a smaller impact on the surrounding environment in front of the running trains, approximately within 70 m and 60 m. With an increase in axle weight, the vibration intensity and propagation range in the vicinity of the railway substantially increase. Therefore, some corresponding vibration isolation measures and relevant vibration control standards can be adopted to improve the living quality of life for workers and residents situated along the railway.

3.5 Comparison analysis of dynamic response

3.5.1 Three direction vibration accelerations

Figure 10 shows the vibration acceleration in three directions of the cutting slope in a mountainous area, with regard to a running C80 train. It is noted that at locations near the track, *Y* direction vibrations are dominant, particularly for the M1 point. Despite this, as the distance from the track increases, the *Y* direction acceleration decreases rapidly and becomes comparable with the *X* direction and *Z* direction accelerations. Within a field 10–30 m from the track, the vibration wave near the slope surface will be reflected and superimposed multiple times, which indicates that the acceleration amplitudes of the three directions are relatively close. At M4, approximate 30 m from the track, the *Y* direction vibration attenuates by more than 80%, and the attenuation rates are 60% and 76%, corresponding to the *X* direction and *Z* direction.

3.5.2 Comparison of the vibration level increment

Compared with the vibration level induced by the

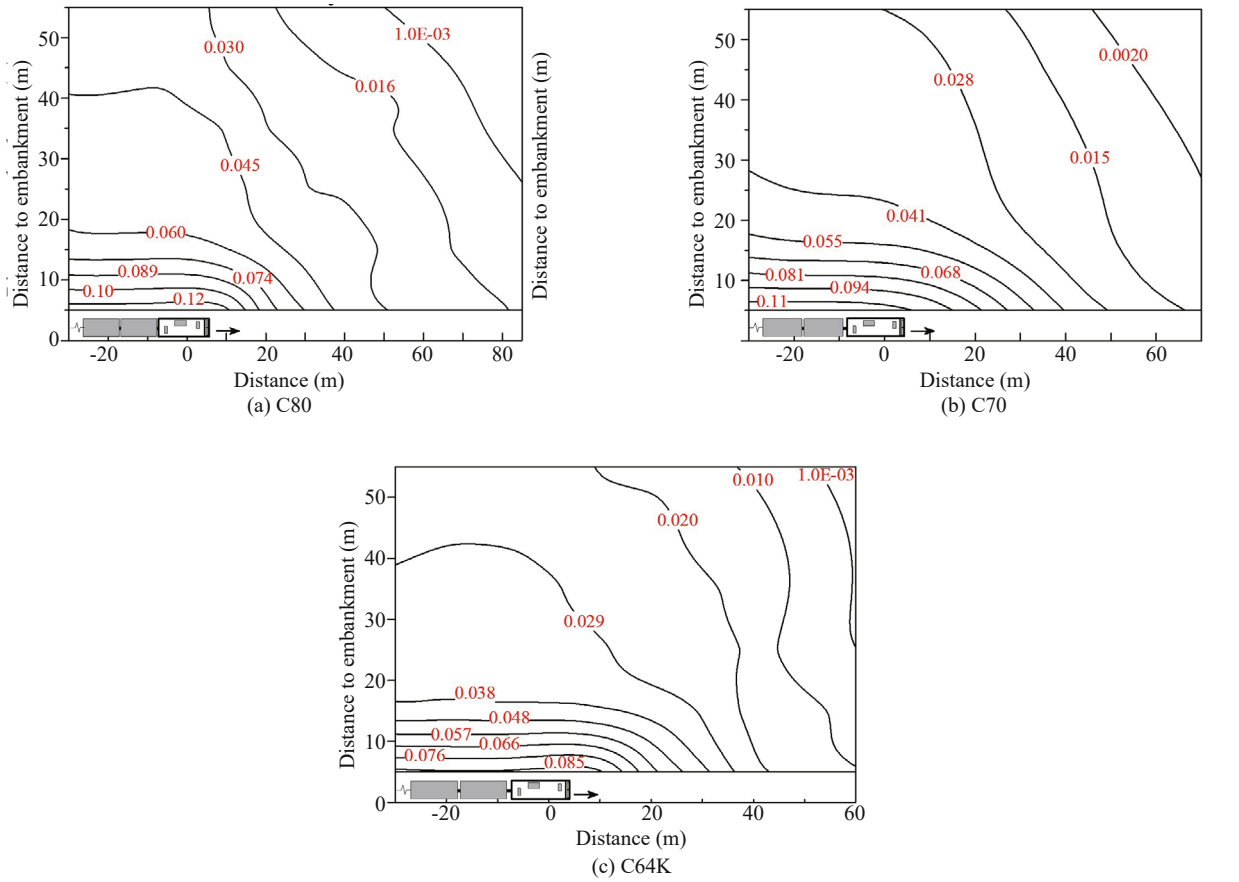

Fig. 9 Vibration affected area induced by trains (unit: m/s²)

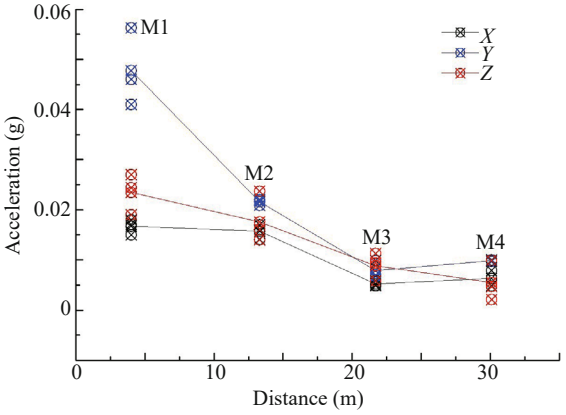

Fig. 10 Three direction accelerations for cutting track

C80 full-load train, it exhibits a distinctly increased amplitude of vibration level, with C80 trains running parallel after meeting. Figure 11 shows the acceleration level increment in the near-field between the embankment and the cutting sections. It can be discerned that the acceleration level increment of the cutting section is relatively larger when the C80 trains run parallel after meeting, due to the multiple diffraction and reflection of the vibration wave in the cutting slope. The difference in acceleration level increments between the embankment and montanic cutting sections are much larger closer to the track, while the difference gradually becomes small as distance increases, especially 20 m away from the track. Additionally, compared to the acceleration level increment in *X* direction, the acceleration level increments of the *Y* direction and *Z* direction are larger, with the increase amplitude varying from 1.2–2.5 dB.

3.5.3 Comparison of three direction accelerations

Figure 12 shows the effect of the earthwork profile configuration on different direction vibrations. The curves show the average value of the acceleration peak for both the embankment and cutting cases. The montanic cutting case generates higher amplitude vibrations in all three directions compared to the embankment case, especially in the area close to the track. But as distance increases, the deviation gradually decreases. Around the 20 m area from the track, the *Y* direction acceleration increases 81% compared to the embankment, and the *X* direction and *Y* direction are 21% and 75%. The vibration acceleration in three directions decays with increased distance to the track, but for the cutting slope, the acceleration decays faster in the near-track area. This is possibly due to the presence of a retaining wall located near the track; the vibration acceleration decays faster in the near field.

4 Train-track-subgrade system model

4.1 Track load model

The load model allows a fully three-dimensional analysis that involves vibrations induced by a heavy-duty railway, taking into account static load and moving load generated by heavy-duty trains, plus the superpositional effects of axles loading. The presented model is based on the vibration source array along the ballast surface, which will propagate in the embankment and foundation soil to generate a vibration incentive effect. This is a particular case that affords the opportunity to study the vibration induced by a heavy-duty railway and to consider the dynamic interaction between sleepers and ballast, using an efficient calculation procedure.

Taking the C80 heavy-duty train as an object, the wheel-rail force that acts on the track is described by the dynamic load equation (Jenkins *et al*., 1974; Liang *et al*., 1999; Li *et al*., 2005; Xu *et al*., 2011):

$$F(t)=\eta_1\eta_2\left(P_0+P_1\sin\theta_1 t+P_2\sin\theta_2 t+P_3\sin\theta_3 t\right) \quad (1)$$

where η_1 = superposition coefficient, the value is 1.54; η_2 = dispersion coefficient, the value is 0.75; P_0 = static load, the value is 125 kN;

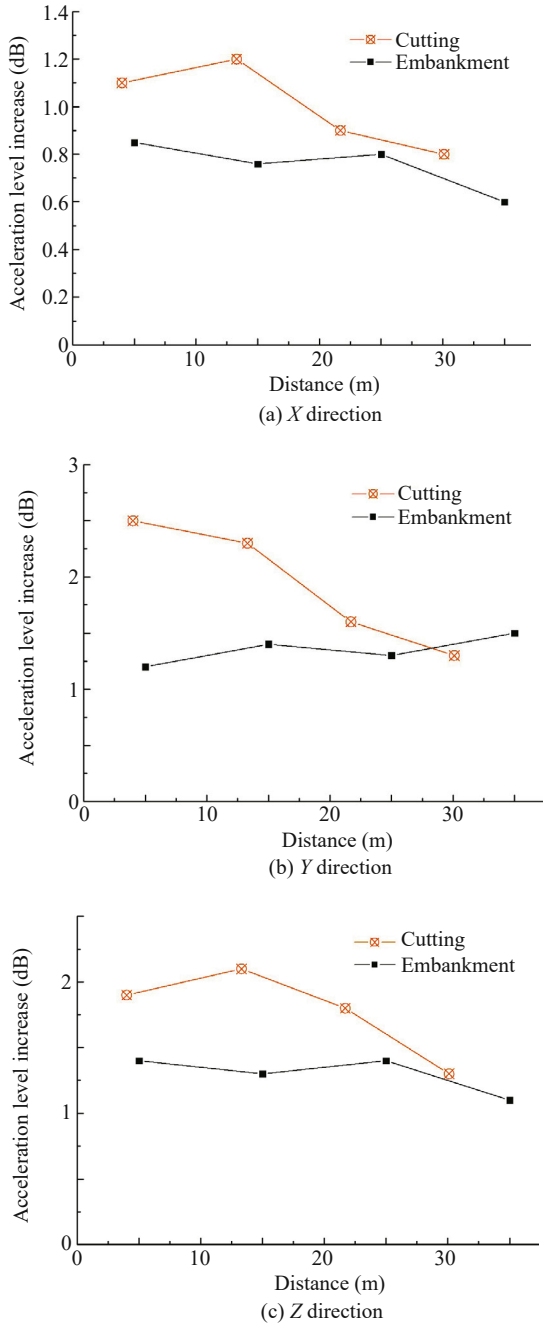

Fig. 11 Comparison analysis of acceleration level increase

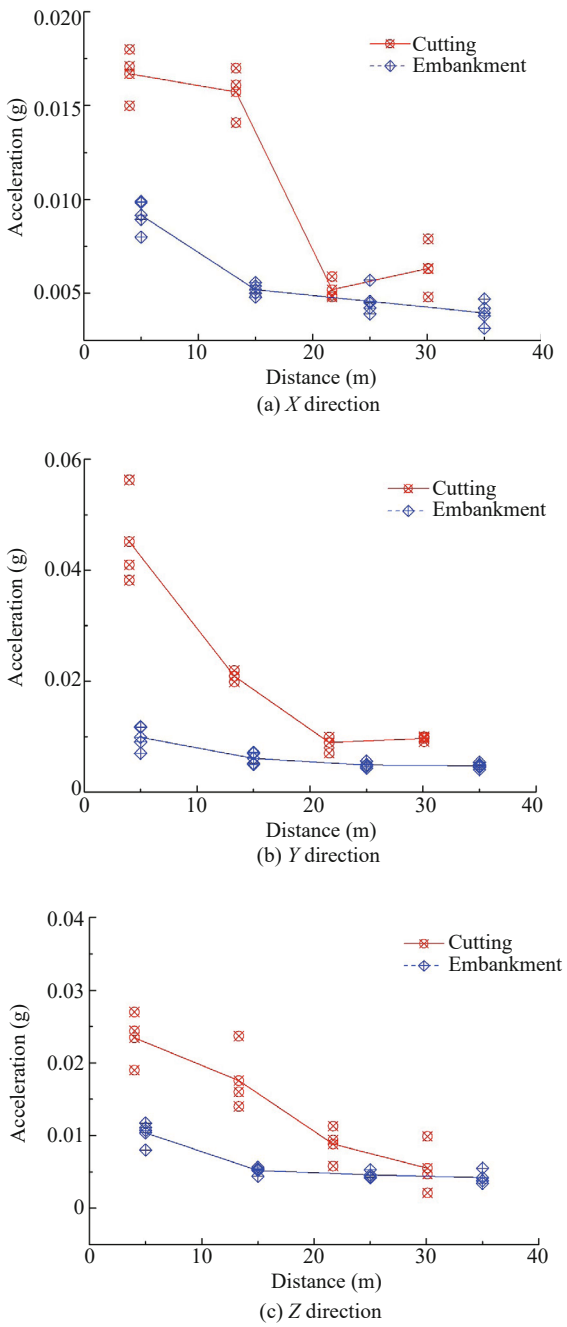

Fig. 12 Comparison analysis of three-direction acceleration

$$P_i = M_0 a_i \theta_i^2 \qquad \theta_i = 2\pi v / L_i \tag{2}$$

where M_0 = unsprung mass; a_i = vector height of the track irregularity; θ_i = vibration circle frequency; v = constant train velocity; L_i = typical wavelength of the track irregularity. This is shown in Table 2.

The heavy-duty train is assumed to have n pairs of wheels and a vertical load column $F_1, F_2, ..., F_n$ generated by each wheel pair. If the load F_1 action position represents the track movement coordinate origin, the vertical deflection $\omega_1(\nabla_1)$ of the point S on the track caused by F_1 can be expressed as:

$$\omega_1(\nabla_1) = \frac{F_1}{8EI\alpha^3\beta} \exp^{-\alpha\beta|\nabla_1|}\left[\cos(\alpha\lambda\nabla_1) + \frac{\beta}{\lambda}\sin(\alpha\lambda|\nabla_1|)\right],$$
$$\nabla_1 = vt - x \tag{3}$$

where $\alpha = (k_s/4EI)^{1/4}$, k_s = spring stiffness of the track, with the value 141.7 MN/m^2; the bending stiffness EI is 7.567×10^6 N·m^2. The model consists of an infinite rectilinear rail-beam characterized by E, I, representing Young′s modulus, the second moment of inertia (Mezeh *et al*., 2019). Since the speed of the heavy-duty train is very small compared with the minimum wave speed of the track-free vibration, the values of β and λ are equal to 1.

Here, a_1 is 1.83 m, a_2 is 8.2 m, a_3 is 10.03 m, and a_4 is 12 m, as shown in Fig. 13(b). Therefore, the vertical deflection caused by the remaining axle load at the point S is described as follows:

$$\omega_2(\nabla_2) = \frac{F_2}{8EI\alpha^3\beta} \exp^{-\alpha\beta|\nabla_2|}\left[\cos(\alpha\lambda\nabla_2) + \frac{\beta}{\lambda}\sin(\alpha\lambda|\nabla_2|)\right],$$
$$\nabla_2 = vt - a_1 - x$$

$$\omega_3(\nabla_3) = \frac{F_3}{8EI\alpha^3\beta} \exp^{-\alpha\beta|\nabla_3|}\left[\cos(\alpha\lambda\nabla_3) + \frac{\beta}{\lambda}\sin(\alpha\lambda|\nabla_3|)\right],$$
$$\nabla_3 = vt - a_2 - x$$
$$\vdots$$
$$\omega_n(\nabla_n) = \frac{F_n}{8EI\alpha^3\beta} \exp^{-\alpha\beta|\nabla_n|}\left[\cos(\alpha\lambda\nabla_n) + \frac{\beta}{\lambda}\sin(\alpha\lambda|\nabla_n|)\right],$$
$$\nabla_n = vt - a_{n-1} - x \tag{4}$$

The vertical deflection caused by the entire train load to the point S represents the superposition effects of each wheel pair action, namely,

$$\omega(\nabla, t) = \sum_{n=1}^{n-1} \frac{F_n}{8EI\alpha^3\beta} \exp^{-\alpha\beta|\nabla_n|}\left[\cos(\alpha\lambda\nabla_n) + \frac{\beta}{\lambda}\sin(\alpha\lambda|\nabla_n|)\right],$$
$$\nabla_n = vt - a_{n-1} - x \tag{5}$$

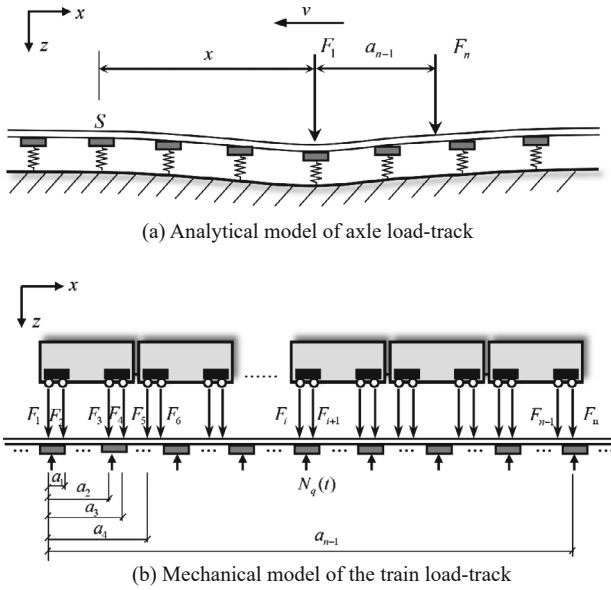

(a) Analytical model of axle load-track

(b) Mechanical model of the train load-track

Fig. 13 Mechanical analysis model

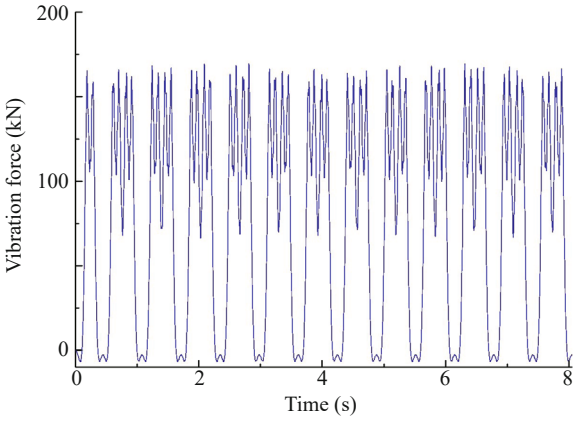

Fig. 14 Force on the ballast layer caused by the C80 heavy-duty train

Table 2 Calculation parameters

Axle load (t)	M_0 (t)	v (km/h)	L_i	a_i
25	1.2	70	10 m	3.5 mm
			2.0 m	0.4 mm
			0.5 m	0.08 mm

Considering the dynamic load function $F(t)$, the force $N_q(t)$ on the ballast layer can be expressed as:

$$N_q(t)=\frac{4F(t)}{\omega_{\text{smax}}}\cdot \sum_{n=1}^{n-1}\frac{F_n}{8EI\alpha^3\beta}\exp^{-\alpha\beta|\nabla_n|}\cdot\left[\cos(\alpha\lambda\nabla_n)+\frac{\beta}{\lambda}\sin(\alpha\lambda|\nabla_n|)\right](d/\xi) \tag{6}$$

where d = sleeper spacing, the value is 0.6 m, $\xi=\pi/\alpha$ is the effective range of track static deflection. ω_{smax} indicates that the maximum static deflection is expressed as:

$$\omega_{\text{smax}}=\frac{F}{8EI\alpha^3\beta} \tag{7}$$

where F = axle load.

Thus, the dynamic load $N_q(t)$ on the ballast layer can be calculated through Eqs. (1) to (7). Figure 14 shows a schematic of an exciting force on the ballast layer caused by the C80 heavy-duty train running at 70 km/h. This load time-history clearly reflects the influence of each axle load on the track. The action caused by the moving axle load is distinct. In the process of numerical model calculation, the vibration force on the ballast layer or the subgrade can act as the excitation vibration source input (Koroma *et al*., 2017; Auersch, 2005; Wu *et al*., 2018; Huang and Chrismer, 2013) in order to study the environmental vibration problem caused by the heavy-duty train.

4.2 Numerical analysis model

The dynamic calculation module in FLAC3D can be used to analyze traffic-induced ground vibration (Mhanna *et al*., 2012; Mezeh *et al*., 2018). Based on the calculated dynamic load $N_q(t)$ of the heavy-duty train acting on the ballast layer, a three-dimensional dynamic model is established by FLAC3D according to the test section of the Shuozhou-Huanghuagang railway line. The height of the embankment is 4.1 m, and the width of the ballast is 11 m. The track model is composed of a 0.6 m-thick gravel ballast layer, a 0.5 m-thick sub-grade, and a 3 m-thick embankment body. The foundation thickness is 20 m, which extends 50 m on both sides of the embankment and 60 m along the track, as shown in Fig. 15.

The finite difference mesh for each element was selected by considering the criterion of numerical accuracy of wave transmission to avoid wave distortion (Dong *et al*., 2018). Based on this criterion, the element size should be smaller than one-eighth to one-tenth of the wavelength of the highest frequency component of the input acceleration wave. In the dynamic calculation process, Rayleigh damping is selected to damp the oscillation and noise due to the low-frequency component. Based on the FLAC3D manual and the natural frequency of dynamic model, the critical damping ratio of 0.5% and the predominant frequency of 2.5 Hz were selected for the dynamic analysis. In addition, the free-field boundary condition was applied on the sides of the model to absorb waves and avoid unwanted wave reflection into the model. Similarly, the absorbing boundary also was needed for the bottom edge of the model to absorb

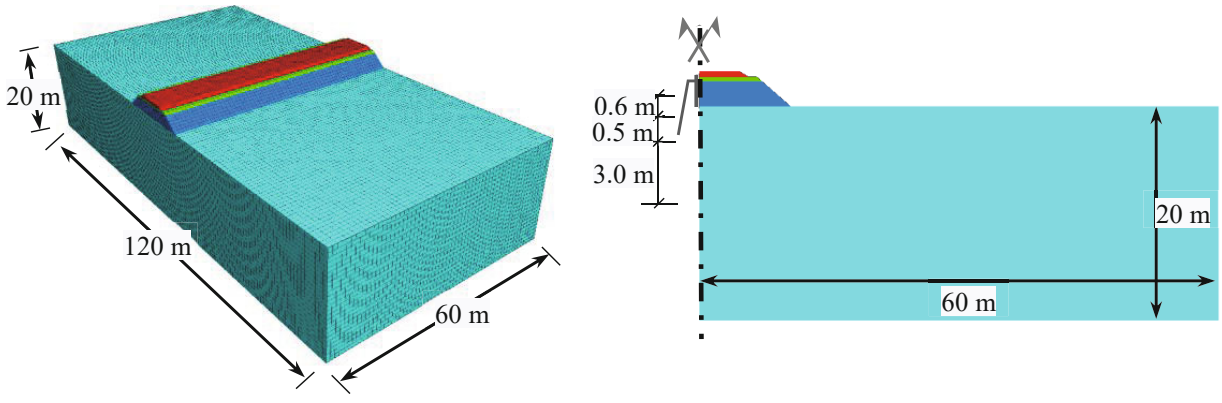

Fig. 15 Numerical calculation model

Table 3 Calculation parameters of the numerical model

Components	E (MPa)	v	ρ (kg/m^3)	C_s (m/s)	d (m)
Ballast	200	0.25	2300	187	0.6
Sub-grade	180	0.25	2200	181	0.5
Embankment	120	0.30	2000	152	3.0
Foundation	100	0.35	1800	143	20

reflecting waves to improve the accuracy of the model analysis. A technique for FLAC3D was developed to perform free field computation analysis parallel to the main grid. The lateral boundaries of the main grid were coupled to the free-field grid by viscous dashpots, and the unbalanced forces from the free-field grid were applied to the main-grid boundary. Thus the free-field boundary could absorb energy to improve the accuracy of the dynamic analysis.

4.2.1 The parameters for the numerical model

The model assumes that the properties of the embankment and the foundation material are uniform along the track. Due to the multiyear operations of heavy-duty trains, the embankment has completely settled. Under the dynamic load of the train, the embankment and foundation in the model will be in their elastic states. With respect to the numerical model, the material constitutive relationships select a linear elastic model; the specific calculation parameters are shown in Table 3.

4.2.2 Validation of the numerical model with field tests

During the calculation of the model, the vibration acceleration response of the surrounding area is monitored, and the peak of the vibration acceleration collected during the C80 train operation is compared to further verify the validity of the calculation performance of the model.

Figure 16(a) shows the acceleration time history of a monitoring point 5 m from the embankment. The peaks of the vertical vibration acceleration are compared to further verify the validity of the calculation performance. Figure 16(b) reflects the variation in the measured and calculated vibration acceleration peaks at different locations from the embankment. As the distance increases, the attenuation law of the acceleration peak curve is similar, and the acceleration peaks of each measurement point show a small amount of difference.

Figure 17(b) shows that the vibration attenuation rules are similar between the simulated and measured results, and that the maximum amplitude difference is 2.8%. Figure 17(a) reflects the acceleration level time-history comparison between the measured and calculated value at 15 m from the embankment. The analysis shows that the measured vibration level ranges from 77–84 dB, and the vibration level of this area is calculated to range from 78–85 dB. The comparison analysis indicates that the difference between the measured value and the calculated value is small, and the results show agreement.

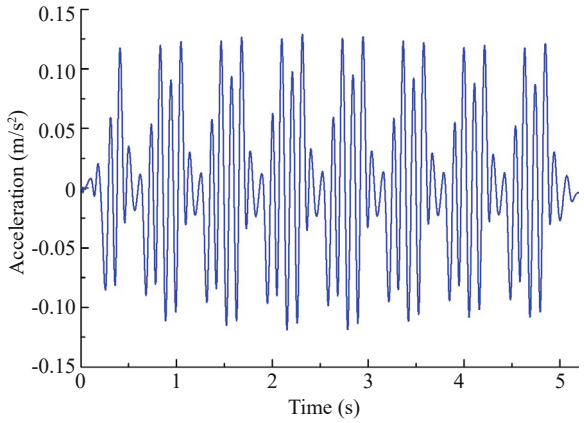

(a) Time-history of vibration acceleration

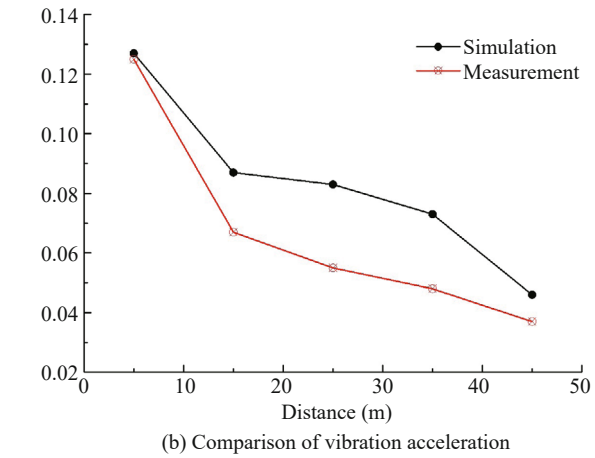

(b) Comparison of vibration acceleration

Fig. 16 Results of numerical simulation

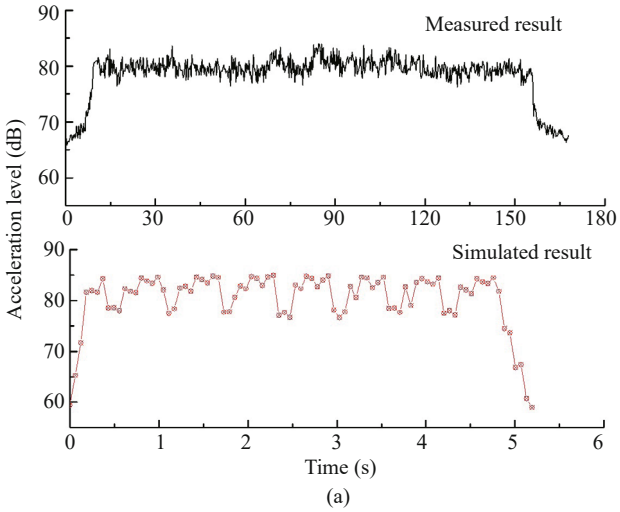

(a)

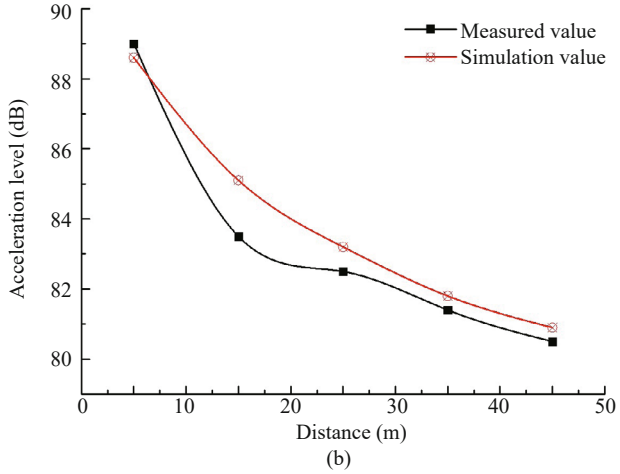

(b)

Fig. 17 Comparison of vibration acceleration level

4.3 Numerical results

To investigate the propagation features of vibration acceleration in the foundation at different depths (-2 m, -7 m, and -12 m), the matrix monitoring points in the vertical section are established specifically to study the acceleration, and the *Y*-direction (perpendicular to the track direction) and *Z*-direction vibration accelerations are specifically examined. The specific monitoring points are shown in Fig. 18.

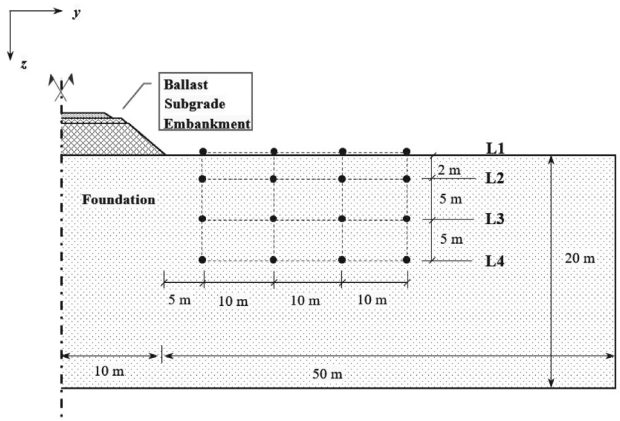

Fig. 18 The monitoring points of vibration acceleration

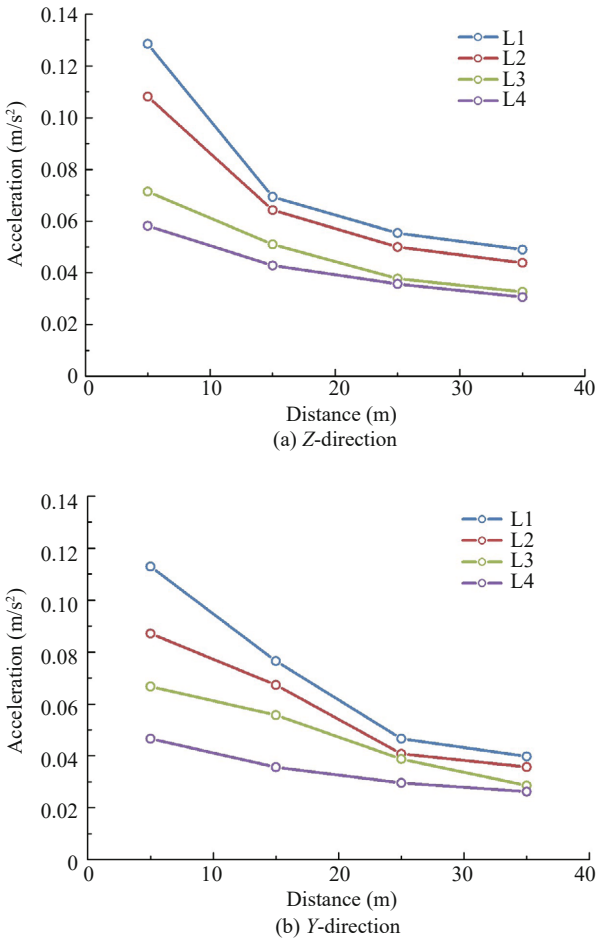

Fig. 19 The attenuation property of the vibration acceleration in the foundation

The attenuation law of acceleration in the foundation is shown in Fig. 19. At greater horizontal distances from the embankment, the acceleration amplitude decreases gradually. As can be seen from Fig. 19(a), in the layer 2(L2), the acceleration close to the embankment is 0.106 m/s^2, and the accelerations of the rest monitoring points are reduced to 0.063 m/s^2, 0.049 m/s^2, and 0.043 m/s^2, respectively, which suggests that the attenuation amplitudes of acceleration are 40.6%, 53.7%, and 59.4%, respectively.

Within 15 m of the embankment, the decay rate of *Z*-acceleration is apparently faster. When the horizontal distance exceeds 15 m, the attenuation rate slowly decreases. A contrast analysis in the vertical direction, when the monitoring point is 5 m from the embankment, shows that acceleration at L4 attenuates by 55.2% more than that monitored at L1. At a horizontal distance 35 m from the embankment, the acceleration of L4 attenuates by 37.7% more than that monitored at L1. Apparently, in the region close to the track, the acceleration decays faster with an increase in depth.

Moreover, when the monitoring point is 5 m closer to the embankment, the *Y*-acceleration at the L4 attenuates by 58.7% more than that monitored at L1. At a horizontal distance of 35 m from the embankment, the *Y*-acceleration of L4 attenuates by 47.5% more than that monitored at L1. Similarly, in the region close to the track, the acceleration decays faster with an increase in depth.

5 Conclusions

Based on the vibration acceleration measurement done on a heavy-duty railway with different track sections situated within a loess area, while combining the train-track-ground dynamic model, the vibration characteristics of the plane region and the multi-stage slope in the mountainous area were contrastively analyzed. The main conclusions are presented as follows:

(1) In the near-field area within 25 m from the embankment, the acceleration peak attenuation was fast, and the vibration amplitude attenuation rates for C80, C70 and C64K trains were 53.1%, 61.8%, 48.8%, respectively. In the far field, 25 m away from the embankment, the acceleration peak attenuation trend gradually decreased. Compared with the embankment section, due to the multi-stage slope of the cutting section, the decay rate of vibration acceleration was faster. At the footing of the third grade soil slope, the acceleration decay rate was 88%.

(2) According to the analysis of the acceleration by the plane matrix test, the C80 train caused the strongest vibration response in the near-field area, and the ground vibration acceleration ranged from 0.13–0.055 m/s^2. The amplitude of the vibration acceleration at the same distance from the embankment was not consistent due to

the inhomogeneity of loess soil. The matrix monitoring points were established in the foundation at different depths. It was found that in the region close to the track, the acceleration decayed faster with an increase in depth.

(3) As the propagating distance increased, the high-frequency portion attenuated faster compared to the low-frequency portion, due to the dissipation of high-frequency energy in the soil medium. In the 5 m area from the track, the frequency band of the vibration by the C80 was mainly distributed between 10–88 Hz, and the frequency bands were 18–98 Hz and 20–81 Hz, corresponding to the C70 and C64K. Moreover, in the 15m area away from the track, the frequency bands were mainly distributed between 10–79 Hz, 14–55 Hz, 12–59 Hz, respectively.

(4) The magnitude of the acceleration level in the plane area decreased as the distance increased from the embankment. When a single C80 train ran, the acceleration level of the near-field plane area ranged from approximately 82.2–89.1 dB. Compared with the embankment section, it can be observed that the acceleration level increment of the cutting section in a mountainous area was much larger when the C80 trains ran parallel after meeting. Additionally, compared to the acceleration level increment in the *X* direction, the acceleration level increments of the *Y* direction and *Z* direction were larger, with the increase amplitude ranging from 1.2–2.5 dB.

(5) As axle weight increased, the intensity and range of the wave propagation around the railway also increased. The C80 train operation caused a larger vibration response on the surrounding environment. The vibration in the area within 85 m in front of the running train was strong. Thus, corresponding measures to reduce vibration and relevant vibration control standards should be undertaken to improve the quality of life for residents and workers along the railway.

(6) With regard to the cutting section in mountainous area, the *Y* direction vibration acceleration was dominant, especially close to the track. As the distance to the track increased, the *Y* direction acceleration rapidly decreased and became comparable with the *X* direction and the *Z* direction acceleration. Within 10–30 m from the track, the acceleration amplitudes of the three directions were relatively close. Additionally, the cutting case generated higher amplitude vibrations in all three different directions compared to the embankment section, but as the distance from the track increased, the deviation between acceleration gradually decreased.

Acknowledgement

This work was supported by the Natural Science Foundation of China (No. 51878242) and the Hebei Natural Science Foundation of China (Nos. E2017404013 and E2020404007).

References

Alves Costa P, Calçada R and Cardoso AS (2012), "Track-Ground Vibrations Induced by Railway Traffic: In-Situ Measurements and Validation of a 2.5D FEM-BEM Model," *Soil Dynamics and Earthquake Engineering*, **32**(1): 111–128.

Auersch L (2006), "Ground Vibration Due to Railway Traffic-the Calculation of the Effects of Moving Static Loads and Their Experimental Verification," *Journal of Sound and Vibration*, **293**(3-5): 599–610.

Auersch L (2005), "The Excitation of Ground Vibration by Rail Traffic: Theory of Vehicle–Track–Soil Interaction and Measurements on High-Speed Lines," *Journal of Sound and Vibration*, **284**(1-2): 103–132.

Cao Z, Cai YQ, Sun HL and Xu CJ (2011), "Dynamic Responses of a Poroelastic Half-Space from Moving Trains Caused by Vertical Track Irregularities," *Int J Numer Anal Methods Geomech*, **35**(7): 761–86.

Connolly DP, Alves Costa P, Kouroussis G, Galvin P, Woodward PK and Laghrouche O (2015), "Large Scale International Testing of Railway Ground Vibrations Across Europe," *Soil Dynamics and Earthquake Engineering*, **71**: 1–12.

Connolly DP, Kouroussis G, Woodward PK Alves Costa P, Verlinden O and Forde MC (2014), "Field Testing and Analysis of High Speed Rail Vibrations," *Soil Dynamics and Earthquake Engineering*, **67**: 102–118.

Connolly DP, Marecki GP, Kouroussis G, Thalassinakis L and Woodward PK (2016), "The Growth of Railway Ground Vibration Problems-A Review," *Science of the Total Environment*, **568**: 1276–1282.

Correia dos Santos N, Barbosa J, Calçada R and Delgado R (2017), "Track-Ground Vibrations Induced by Railway Traffic: Experimental Validation of a 3D Numerical Model," *Soil Dynamics and Earthquake Engineering*, **97**: 324–344.

Correia Dos Santos N, Colaço A, Alves Costa P and Calçada R (2016), "Experimental Analysis of Track-Ground Vibrations on a Stretch of the Portuguese Railway Network," *Soil Dynamics and Earthquake Engineering*, **90**: 358–380.

Degrande G and Schillemans L (2001), "Free Field Vibrations During the Passage of a Thalys High Speed Train at Varible Speed," *Journal of Sound and Vibration*, **247**(1): 131–144.

Dong J, Wu ZH, Li X and Chen HY (2018), "Dynamic Response and Pile-Soil Interaction of a Heavy-Haul Railway Embankment Slope Reinforced by Micro-Piles," *Computers and Geotechnics*, **100**: 144–157.

Dong J, Yang Y and Wu ZH (2019), "Propagation Characteristics of Vibrations Induced by Heavy-Haul Trains in a Loess Area of the North China Plains," *Journal of Vibration and Control*, **25**(4): 882–894.

Feng SJ, Zhang XL, Wang L, Zheng QT, Du FL and Wang ZL (2017), "In Situ Experimental Study on High Speed Train Induced Ground Vibrations with the Ballast-Less Track," *Soil Dynamics and Earthquake Engineering*, **102**: 195–214.

Galvín P and Domínguez J (2007), "Analysis of Ground Motion due to Moving Surface Loads Induced by High-Speed Trains," *Engineering Analysis with Boundary Elements*, **31**(11): 931–941.

Gao Y, Huang H, Ho CL and Hyslip JP (2017), "High Speed Railway Track Dynamic Behavior near Critical Speed," *Soil Dynamics and Earthquake Engineering*, **101**: 285–294.

Gao Y, Huang H, Ho CL and Judge A (2018), "Field Validation of a Three-Dimensional Dynamic Track-Subgrade Interaction Model," *Proceedings of the Institution of Mechanical Engineers, Part F: Journal of Rail and Rapid Transit*, **232**(1): 130–143.

Germonpré M, Degrande G and Lombaert G (2017), "A Study of Modelling Simplifications in Ground Vibration Predictions for Railway Traffic at Grade," *Journal of Sound and Vibration*, **406**: 208–223.

Huang H and Chrismer S (2013), "Discrete Element Modeling of Ballast Settlement Under Trains Moving at "Critical Speeds"," *Construction and Building Materials*, **38**: 994–1000.

Jenkins HH, Stephenson JE, Clayton GA, Morland GW and Lyon D (1974), "The Effect of track and Vehicle Parameters on Wheel/Rail Vertical Dynamic Loads," *Journal of Railway Engineering Society*, **3**(1): 2–16.

Karlström A (2006), "An Analytical Model for Ground Vibrations from Accelerating Trains," *Journal of Sound and Vibration*, **293**(3-5): 587–598.

Koroma SG, Thompson DJ, Hussein MFM and Ntotsios E (2017), "A Mixed Space-Time and Wavenumber-Frequency Domain Procedure for Modelling Ground Vibration from Surface Railway Tracks," *Journal of Sound and Vibration*, **400**: 508–532.

Kouroussis G, Pauwels N, Brux P, Conti C and Verlinden O (2014), "A Numerical Analysis of the Influence of Tram Characteristics and Rail Profile on Railway Traffic Ground-Borne Noise and Vibration in the Brussels Region," *Science of the Total Environment*, **482-483**: 452–460.

Li J, Chen SX, Yu F and Dai ZJ (2018), "Remote Monitoring for a High-Speed Railway Subgrade Structure State in a Mountainous Area and Its Response Analysis," *Bulletin of Engineering Geology and the Environment*, **77**(1): 409–427.

Li L, Zhang BQ and Yang XL (2005), "Analysis of Dynamic Response of Large Cross-Section Tunnel Under Vibration Load Induced by High Speed Train," *Chinese Journal of Rock Mechanics and Engineering*, **23**: 4259–4265. (in Chinese)

Li P, Ling XZ, Zhang F and Li Y (2017), "Field Testing and Analysis of Embankment Vibrations Induced by Heavy Haul Trains," *Shock and Vibration*, **2017**: 1–14.

Liang B and Cai Y (1999), "Dynamic Analysis of Subgrade of High Speed Railways in Geometric Irregular Condition," *Journal of the China Railway Society*, **21**(2): 84–88. (in Chinese)

Ling XZ, Zhang F, Zhu ZY, Ding L and Hu QL (2009), "Field Experiment of Subgrade Vibration Induced by Passing Train in a Seasonally Frozen Region of Daqing," *Earthquake Engineering and Engineering Vibration*, **8**(1): 149–157.

Lombaert G, Galvín P and François S (2014), "Quantification of Uncertainty in the Prediction of Railway Induced Ground Vibration Due to the Use of Statistical Track Unevenness Data," *Journal of Sound and Vibration*, **333**(18): 4232–4253.

Lu F, Gao Q, Lin JH and Williams FW (2006), "Non-Stationary Random Ground Vibration Due to Loads Moving Along a Railway Track," *Journal of Sound and Vibration*, **298**(1-2): 30–42.

Mezeh R, Mroueh H, Hosseingholian M and Sadek M (2019), "New Approach for the Assessment of Train/Track/Foundation Dynamics Using in-Situ Measurements of High-Speed Train Induced Vibrations," *Soil Dynamics and Earthquake Engineering*, **116**: 50–59.

Mezeh R, Sadek M, Chehade FH and Mroueha H (2018), "Adaptive Meshing Scheme for Prediction of High-Speed Moving Loads Induced Ground Vibrations," *Computers and Geotechnics*, **100**: 188–202.

Mezeh R, Sadek M, Chehade FH and Shahrour I (2017), "Adaptive analysis of Infinite Beams Dynamics Problems Using the Periodic Configuration Update Method in the Time Domain," *International Journal for Numerical and Analytical Methods in Geomechanics*, **42**(4): 618–635.

Mhanna M, Sadek M and Shahrour I (2012), "Numerical Modeling of Traffic-Induced Ground Vibration," *Computers and Geotechnics*, **39**: 116–123.

Picoux B and Houédec DL (2005), "Diagnosis and Prediction of Vibration from Railway Trains," *Soil Dynamics and Earthquake Engineering*, **25**(12): 905–921.

Sheng X, Jones C and Petyt M (1999), "Ground Vibration Generated by a Harmonic Load Acting on a Railway Track," *Journal of Sound and Vibration*, **225**: 3–28.

Sheng X, Jones CJC and Thompson DJ (2003), "A Comparison of a Theoretical Model for Quasi-Statically and Dynamically Induced Environmental Vibration from Trains with Measurements," *Journal of Sound and Vibration*, **267**(3): 621–635.

Sun LM, Xie WP, He XW and Hayashikawa T (2016), "Prediction and Mitigation Analysis of Ground Vibration Caused by Running High-Speed Trains on Rigid-Frame Viaducts," *Earthquake Engineering and Engineering Vibration*, **15**(1): 31–47.

Taga H, Turkmen S and Kacka N (2015), "Assessment of Stability Problems at Southern Engineered Slopes Along Mersin-Tarsus Motorway in Turkey," *Bulletin of Engineering Geology and the Environment*, **74**(2): 379–391.

Wang FT, Tao XX, Xie LL and Siddharthan R (2017), "Green's Function of Multi-Layered Poroelastic Half-Space for Models of Ground Vibration due to Railway Traffic," *Earthquake Engineering and Engineering Vibration*, **16**(2): 311–328.

Wu ZJ, Chen T, Zhao T and Wang LL (2018), "Dynamic Response Analysis of Railway Embankments Under Train Loads in Permafrost Regions of the Qinghai-Tibet Plateau," *Soil Dynamics and Earthquake Engineering*, **112**: 1–7.

Xia H, Chen JG, Wei PB, Xia CY, De Roeck G and Degrande G (2009), "Experimental Investigation of Railway Train-Induced Vibrations of Surrounding Ground and a Nearby Multi-Story Building," *Earthquake Engineering and Engineering Vibration*, **8**(1): 137–148.

Xia H, Cao YM and Roeck GD (2010), "Theoretical Modeling and Characteristic Analysis of Moving-Train Induced Ground Vibrations," *Journal of Sound and Vibration*, **329**(7): 819–832.

Xu HQ, Fu ZF, Liang LG, Wang GB and Chen L (2011), "Ambient vibration analysis of Adjacent Perpendicular Multi-Tunnels Under Train Loads," *Rock and Soil Mechanics*, **32**(6): 1869–1874. (in Chinese)

Yang YB, Hung HH and Chang DW (2003), "Train-Induced Wave Propagation in Layered Soils Using Finite/Infinite Element Simulation," *Soil Dynamics and Earthquake Engineering*, **23**(4): 263–278.

Zhai WM, He ZX and Song XL (2010), "Prediction of High-Speed Train Induced Ground Vibration Based on Train-Track-Ground System Model," *Earthquake Engineering and Engineering Vibration*, **9**(4): 545–554.

Zhai WM, Wei K, Song XL and Shao MH (2015), "Experimental Investigation into Ground Vibrations Induced by Very High Speed Trains on a Non-Ballasted Track," *Soil Dynamics and Earthquake Engineering*, **72**: 24–36.

Zhang ZH, Zhang XD, Qiu HS and Daddow M (2016), "Dynamic Characteristics of Track-Ballast-Silty Clay with Irregular Vibration Levels Generated by High-Speed Train Based on DEM," *Construction and Building Materials*, **125**: 564–573.